Geomechanical aspects of CO_2 sequestration in a deep saline reservoir in the Ohio River Valley region

Amie Lucier, Mark Zoback, Neeraj Gupta, and T. S. Ramakrishnan

ABSTRACT

The Ohio River Valley CO_2 Storage Project is an ongoing characterization of deep saline formations being considered as potential sites for geological CO_2 sequestration. We completed a geomechanical analysis of the Rose Run Sandstone, a potential injection zone, and its adjacent formations at the American Electric Power's 1.3-GW Mountaineer Power Plant in New Haven, West Virginia. The results of this analysis were then applied to three investigations used to evaluate the feasibility of anthropogenic CO_2 sequestration in the potential injection zone. First, we incorporated the results of the geomechanical analysis with a geostatistical aquifer model in CO_2 injection-flow simulations to test the effects of introducing a hydraulic fracture to increase injectivity. We observed a nearly fourfold increase of injection rate caused by the introduction of a hydraulic fracture in the injection zone. The flow simulations predict that a single vertical well with a hydraulic fracture could inject a maximum of 300–400 kt of CO_2/yr. In the second investigation, we determined that horizontal injection wells at the Mountaineer site are feasible because the high rock strength ensures that such wells would be stable in the local stress state. The third investigation used the geomechanical analysis results to evaluate the potential for injection-induced seismicity. If preexisting, but undetected, nearly vertical faults striking north-northeast or east-northeast are present, the increased pore pressure from CO_2 injection would raise their reactivation potential. Geomechanical analysis of potential CO_2 sequestration sites provides critical information required to evaluate its sequestration potential and associated risks.

DOI:10.1306/eg.11230505010

AUTHORS

AMIE LUCIER ~ *Department of Geophysics, Stanford University, Stanford, California 94305; luciera@pangea.stanford.edu*

Amie Lucier is a Ph.D. candidate in geophysics at Stanford University. She is a research assistant in the Stress and Crustal Mechanics Group investigating geomechanical questions related to CO_2 sequestration, mining, and the petroleum industry. She received her M.S. degree (2004) in geophysics from Stanford University and her B.S. degree (2002) in geology from Washington and Lee University.

MARK ZOBACK ~ *Department of Geophysics, Stanford University, Stanford, California 94305*

Mark Zoback is the Benjamin M. Page Professor of Earth Sciences and professor of geophysics at Stanford University. His principal research interests are related to the forces that act within the Earth's crust and their influence on processes related to plate tectonics, earthquakes, oil and gas reservoirs, and CO_2 sequestration.

NEERAJ GUPTA ~ *Battelle Memorial Institute, 505 King Ave., Columbus, Ohio 432201-2693*

Neeraj Gupta is a research leader in the Environmental Technology Department at the Battelle Memorial Institute, Columbus, Ohio. He received a Ph.D. in hydrogeology from Ohio State University, an M.S. degree in geochemistry from George Washington University, and M.Sc. and B.Sc. degrees in geology from Panjab University, India. He has been leading Battelle's research on CO_2 sequestration and also maintains active interest in groundwater characterization, modeling, and remediation research.

T. S. RAMAKRISHNAN ~ *Schlumberger-Doll Research, 36 Old Quarry Rd., Ridgefield, Connecticut 06877*

T. S. Ramakrishnan is a scientific advisor in Schlumberger-Doll Research and is currently responsible for carbon sequestration research within Schlumberger. He has published in the areas of two-phase flow in porous media, well testing, enhanced oil recovery, carbonate rock physics, invasion, relative permeability logging, formation testers, intelligent completions, etc. He has a B.Tech. degree (Indian Institute of Technology, Delhi) and a Ph.D. (Illinois Institute of Technology, Chicago) in chemical engineering.

ACKNOWLEDGEMENTS

We thank Phil Jagucki, Frank Spane, Joel Sminchak, and Danielle Meggyesy of Battelle Memorial Institute and Austin Boyd and Nadja Muller of Schlumberger, for their contributions in the collection and analysis of field data, and Kristian Jessen and Taku Ide of the Petroleum Engineering Department at Stanford University, for their help with the flow simulations. We thank GeoMechanics International for the use of their software. Funding for this study was provided through Stanford University's Global Climate and Energy Project. Funding for the Ohio River Valley CO_2 Storage Project was provided by the U.S. Department of Energy's Office of Fossil Energy through the National Energy Technology Laboratory. Other sponsors include the American Electric Power, BP, Ohio Coal Development Office of the Ohio Air Quality Development Office, Battelle, Pacific Northwest National Laboratory, and Schlumberger.

INTRODUCTION

In regions like the Ohio River Valley that have many large point sources of CO_2 emissions and limited options for CO_2 sequestration in other geological media, such as oil and gas reservoirs, the feasibility evaluation of CO_2 sequestration in deep saline aquifers is essential. Within the states of West Virginia, Ohio, Pennsylvania, Kentucky, Illinois, and Indiana, annual CO_2 emissions from power plants reached nearly 700 Mt in 2000. More than 98% of these emissions were from 185 coal-burning power plants (Figure 1a). According to the Environmental Protection Agency's (EPA, 2002) eGRID2002 database, 108 of the 185 coal plants emitted more than 1 Mt CO_2/yr, with 22 emitting more than 10 Mt CO_2/yr (2002). Locating CO_2 sequestration sites in close proximity to large point sources such as these can significantly reduce the total cost of sequestration by minimizing the associated transportation costs. Failure to find sites with acceptable storage capacity in the vicinity of these CO_2 sources could make geological sequestration an impractical option for mitigating greenhouse gas emissions in a large part of the conterminous United States.

Finding sequestration capacity in the region is of great importance, but it is equally necessary to ascertain the safety of potential sequestration sites. If the potential for and risk of CO_2 leakage is significant, a site will not be considered any further, even if it possesses the needed capacity. One important aspect of assessing the risk associated with CO_2 sequestration is to understand the tectonic setting and state of stress at a potential sequestration site. Regionally, the Ohio River Valley is located in a relatively stable, intraplate tectonic setting. In general, the regional stress state is strike-slip to reverse faulting, with the maximum horizontal stress (S_{Hmax}) oriented northeast to east-northeast (Figure 1b) (Zoback and Zoback, 1989). Earthquakes in this region are uncommon, but they do occur. Figure 1b indicates the locations of seismic events that have occurred in the region throughout the last 40 yr (black circles). The presence of seismic activity, both natural and induced, is of great importance when evaluating CO_2 sequestration potential. Extensive fault zones may provide leakage pathways along which CO_2 could migrate. The injection of large volumes of CO_2 into a deep aquifer will result in an increase in pore pressure by several megapascals in and around the injection zone, especially during the injection period. This pressure change can lead to slip on preexisting faults when the state of stress is near frictional equilibrium, which is commonly the case in intraplate regions (Townend and Zoback, 2000). Quantifying the localized stress state and fault orientations at potential CO_2 sequestration sites provides the necessary information to assess safe injection pressures and to understand the possibility of CO_2 injection inducing seismicity for specific injection sites.

The Ohio River Valley CO_2 Storage Project seeks to evaluate the potential of deep saline aquifer sequestration at the site of one of the large point sources discussed above (Gupta et al., 2005). Specifically,

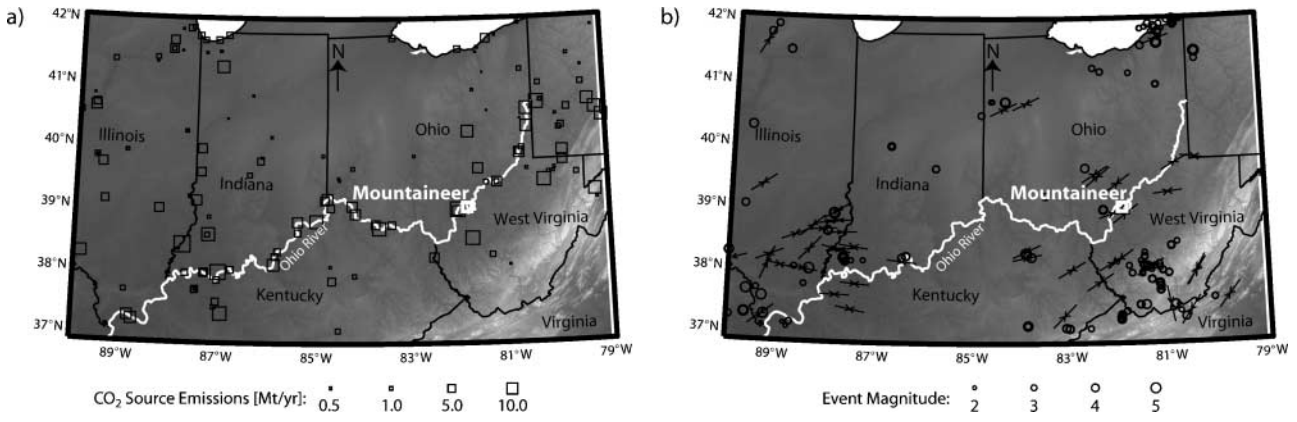

Figure 1. Regional map of the Ohio River Valley. The Ohio River is shown in white. (a) Power plants are shown by squares scaled by the total CO_2 emissions for each site in 2000. The Mountaineer site is indicated in white. (b) The tectonic setting is illustrated with S_{Hmax} stress orientations (inverted arrows) and seismic events since 1964 (circles). The regional S_{Hmax} orientation trends approximately northeast-southwest (Zoback and Zoback, 1989).

this project focuses on a site-specific characterization of the subsurface beneath American Electric Power's (AEP) 1.3-GW Mountaineer Power Plant in New Haven, West Virginia, which emitted 7.2 Mt of CO_2 in 2000 (Figure 1). The evaluation of this site is based on data collected from a seismic reflection survey, geophysical logging and well testing of a 2800-m (9100-ft) (below ground surface) vertical borehole (AEP 1 well), and regional field data. A schematic diagram of the Mountaineer site is depicted in Figure 2, showing the AEP 1 well at depth and in relation to the Mountaineer Power Plant.

During the site characterization, several potential injection zones were identified based on permeability and porosity logs (Figure 3). Out of these, three zones were selected for further assessment (Gupta et al., 2005). Two zones are located in dolomites with secondary permeability and porosity. One of these is at a depth of about 2260 m (7414 ft) in the Ordovician Beekmantown Dolomite, and the other is in the Cambrian Copper Ridge Dolomite at about 2490 m (8169 ft). The third zone is in the Ordovician Rose Run Sandstone from about 2355 to 2388 m (7726 to 7834 ft). The permeability, determined from a nuclear magnetic resonance (NMR) transverse relaxation log, is less than 1 md for much of the borehole but occasionally peaks to about 50–100 md in selected sections. We also analyzed preexisting fractures in the potential injection zones as a source of effective permeability. Using an electrical image log that measures formation microresistivity, we identified the natural fractures that intersect the borehole and determined the strike, dip, and aperture of the fractures. However, we found that natural fractures do not appear to significantly increase permeability. The effective porosity ranges from about 0 to 10%, with a mean porosity of 2.8%. The zones identified as possible injection sites have average effective porosities ranging from 4.1 to 6.9%.

The fact that possible injection zones in deep sedimentary basins such as the Appalachian basin appear to have low to moderate permeability and porosity reinforces the need to understand the geomechanical influences that will guide any reservoir-stimulation techniques. This study focuses on the Rose Run Sandstone as a potential injection zone. We completed a geomechanical analysis of the site and incorporated the results into CO_2 injection-flow simulations. Carbon dioxide injection simulations in three-dimensional (3-D) Rose Run Sandstone reservoir models were used to investigate the effectiveness of hydraulic fracturing to increase injectivity. Another option being considered to increase injectivity is the drilling of deviated and horizontal wells; therefore, we looked at the stability of various well orientations in the given stress field. Finally, we made a preliminary examination of the pressure conditions and fault orientations that, if present, would increase the potential of induced seismicity in the cap rock.

BUILDING A GEOMECHANICAL MODEL

From a geomechanical standpoint, a suitable site for CO_2 sequestration must have sufficient injectivity while maintaining cap rock integrity. The cap rock

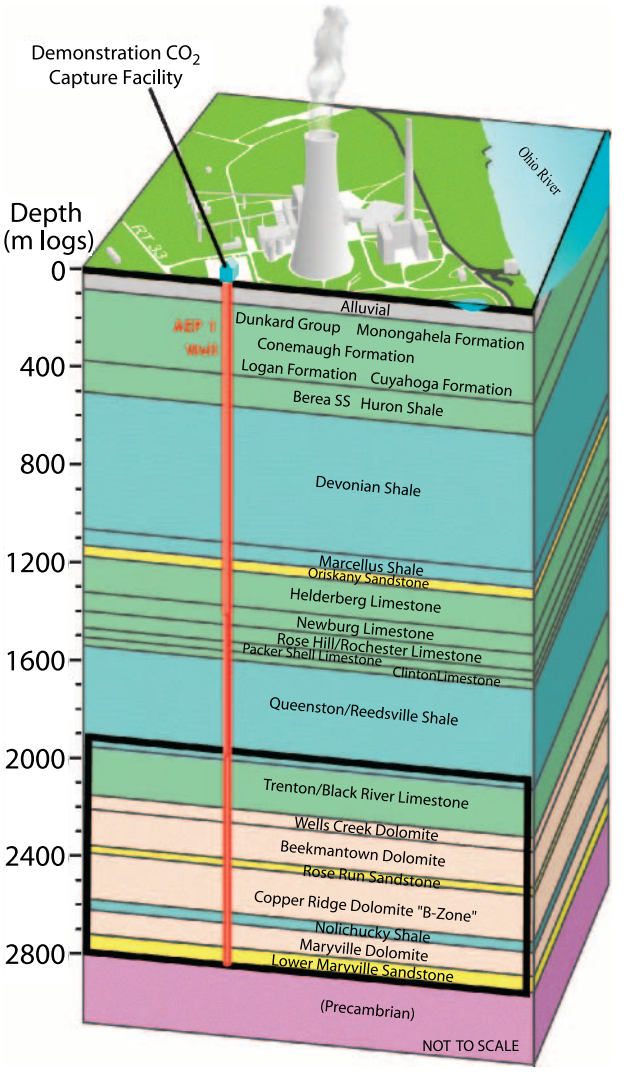

Figure 2. A 3-D schematic of the characterization site at the Mountaineer power plant. The diagram illustrates the well location relative to the power plant and the general stratigraphy intersected by the well. The black box outlines the depths focused on in this article.

must not be susceptible to hydraulic fracture propagation, and the formation itself should be resistant to fault slippage. A suitable sequestration site must also have a cap rock capable of resisting the buoyancy-driven flow of CO_2, so that the fluid can be stored throughout appreciable time scales (hundreds to thousands of years) without leaking. In the geographical region and geological setting of this study, we foresee that reservoir stimulation that preserves the efficacy of the cap rock will be necessary for cost-effective sequestration. Because successful reservoir stimulation requires knowledge of the in-situ stresses, we completed a geomechanical characterization of the Mountaineer site.

The goal of our analysis was to quantify the magnitude and orientation of the three principal stresses and determine whether the stress state affects the viability of the Rose Run Sandstone to act as an effective CO_2 storage unit. The three principal stresses are the vertical stress (S_v) and the minimum and maximum horizontal stresses (S_{hmin} and S_{Hmax}). Our methodology for determining the in-situ stress state followed Zoback et al. (2003):

1. Calculate elastic moduli from velocity and density logs
2. Calculate the vertical stress (S_v) by integrating the density log
3. Identify the occurrence of drilling-induced tensile fractures and wellbore breakouts using electrical image log and caliper data to determine stress orientation

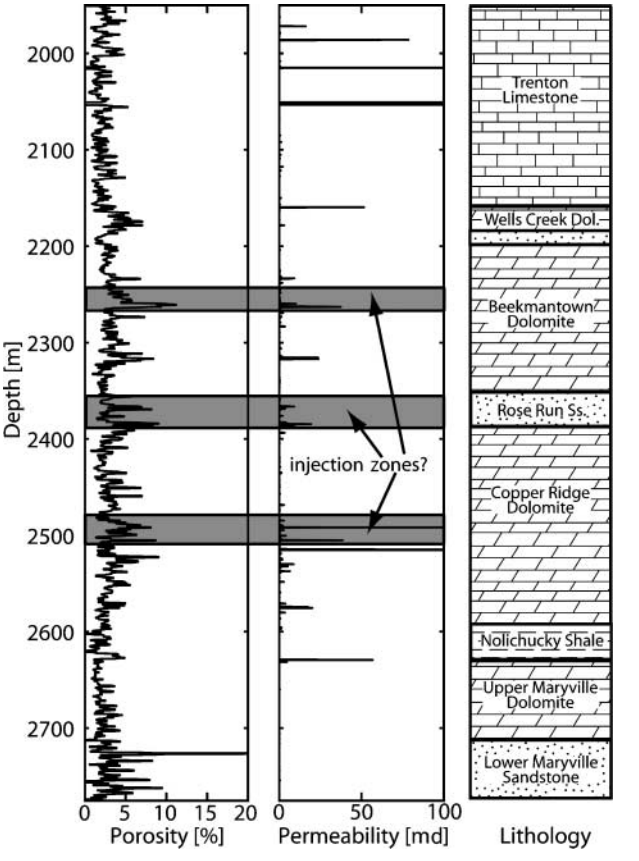

Figure 3. Density-porosity log and NMR permeability log from the AEP 1 well (processed with a median filter of order $N = 9$). The general lithology is shown to the right. Three possible injection zones are highlighted in gray.

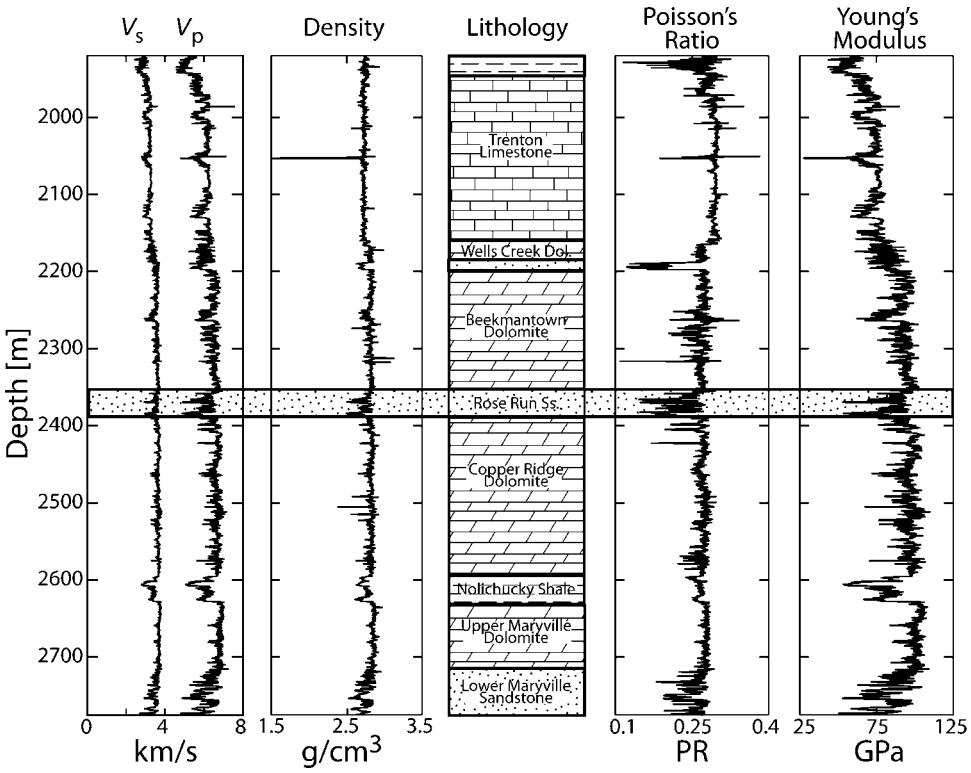

Figure 4. Velocity and density logs from AEP 1 and the calculated Poisson's ratio and Young's modulus. A generalized lithology is shown for reference.

4. Use uniaxial compressive strength (C_o) from core samples to analyze compressive wellbore failures
5. Interpret minifrac tests to determine allowable range of S_{hmin} magnitudes and pore pressure (P_p)
6. Interpret available data to constrain the possible values of S_{Hmax}

Once the state of stress was determined, we used the information to obtain safe injection pressures, model a hydraulic fracture to enhance injectivity, analyze horizontal well stability, and investigate the possibilities of induced seismicity at the site.

Calculation of Elastic Moduli

We used the P- and S-wave velocity logs and the density log from the suite of geophysical logs available from the AEP 1 well to evaluate the Poisson's ratio and Young's modulus associated with different lithologies. Poisson's ratio (ν) is calculated from the following relationship between the P-wave velocity (V_P) and the S-wave velocity (V_S):

$$\nu = \frac{V_P^2 - 2V_S^2}{2(V_P^2 - V_S^2)} \quad (1)$$

Young's modulus (E) is then calculated from rock density (ρ), V_S, and ν:

$$E = 2\rho V_S^2(1 + \nu) \quad (2)$$

The geophysical logs and the results of the elastic moduli calculations are shown along with the general lithology of the well in Figure 4. In the Rose Run Sandstone, V_P decreases significantly more than V_S relative to the adjacent dolomite formations accounting for the sandstone's lower ν value. Along with the decrease in ν in the Rose Run Sandstone, the lower values of V_S and ρ in the sandstone result in a lower E. Poisson's ratio and Young's modulus are material property inputs used in a later section to constrain the possible S_{Hmax} magnitudes allowable under the Mohr-Coulomb criterion for frictional strength.

Vertical Stress Determination

To characterize the in-situ state of stress, we determined the orientation and magnitude of the three, mutually orthogonal, principal stresses. We assumed that one of the principal stresses has a nearly vertical orientation (within 5°), such that the magnitude of

this vertical stress is determined by the weight of the overlying rock material. This assumption was validated by observations of drilling-induced tensile fractures as discussed below. We calculated the magnitude of S_v by integrating the density log throughout the depth of the well:

$$S_v = \int \rho(z) g dz \approx \sum \rho_{avg} g \Delta z \qquad (3)$$

where ρ is rock density, g is gravity acceleration, z is depth, and ρ_{avg} is the average density throughout the depth interval Δz. Figure 5 shows the density log throughout the entire depth range of the well and a plot of depth vs. S_v as determined from the density log. The shallowest 75 m (246 ft) of the density log is extrapolated with a cubic equation to account for the presence of low-density, Cenozoic, unconsolidated, alluvial sediments. The interpolation between 550 and 1191 m (1804 and 3907 ft) is linear. The gradient of S_v with depth determined from a linear fit to the density integration is 26.2 MPa/km. A typical overburden gradient is about 23 MPa/km, but the relatively high density and low porosity of the overburden material at this site result in a higher gradient.

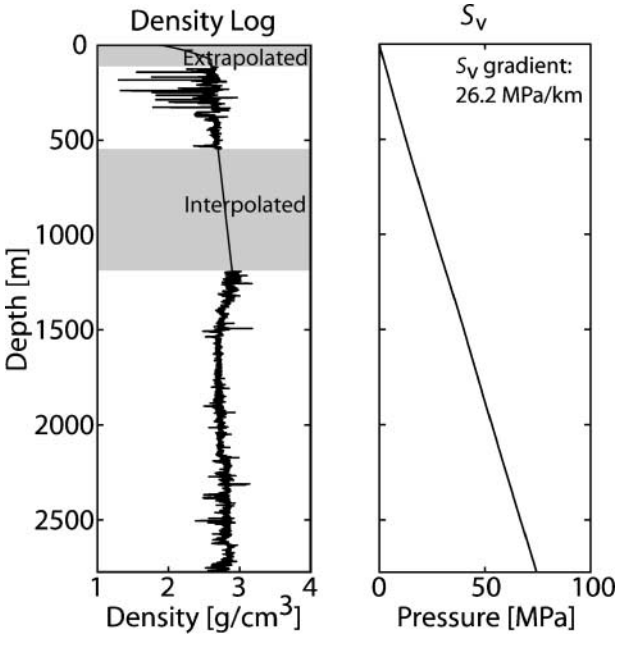

Figure 5. Density log and calculated vertical stress (S_v) magnitude with depth. At some depth intervals, the density was extrapolated or interpolated to compensate for data gaps. The S_v gradient is 26.2 MPa/km.

Determination of Stress Orientation

As a well is drilled, stress is concentrated at the wellbore wall. This stress concentration is described by the well-known Kirsch equations (Kirsch, 1898). In a vertical well, the effective stresses at the wellbore wall are described as the hoop stress ($\sigma_{\theta\theta}$), the radial stress (σ_{rr}), and the stress parallel to the wellbore wall (σ_{zz}) (Jaeger and Cook, 1979):

$$\sigma_{\theta\theta} = S_{hmin} + S_{Hmax} - 2(S_{Hmax} - S_{hmin})\cos(2\theta) - 2P_p - \Delta P - \sigma^{\Delta T} \qquad (4)$$

$$\sigma_{rr} = \Delta P \qquad (5)$$

$$\sigma_{zz} = S_v - 2\nu(S_{Hmax} - S_{hmin})\cos(2\theta) - P_p - \sigma^{\Delta T} \qquad (6)$$

where θ is the angle around the hole measured from the azimuth of S_{Hmax}, P_p is the pore pressure, ΔP is the difference between wellbore pressure (resulting from the weight of the drilling mud column) and P_p, $\sigma^{\Delta T}$ is the thermal stress induced by cooling of the wellbore by ΔT degrees, and ν is the static Poisson's ratio. In certain in-situ stress states, the stress concentration may lead to tensile failure along the wellbore wall, creating drilling-induced fractures and/or compressional failure, resulting in breakouts. Drilling-induced tensile fractures occur where the effective stress components, commonly the hoop stress, becomes negative and equal in magnitude to the tensile strength T_o of the rock; breakouts occur where the one of the stress components reaches a maximum and exceeds the compressive strength C_o (Figure 6a) (Zoback et al., 2003).

Moos and Zoback (1990) demonstrated that in the absence of excessive mud weights or of wellbore cooling during drilling, drilling-induced tensile fractures are most likely to form in vertical wells when the state of stress is in a strike-slip regime, such that S_v is the intermediate principal stress, and there is high horizontal stress anisotropy ($S_{hmin} < S_v < S_{Hmax}$). They may also form when the stress state is nearly strike slip, such that the magnitude of S_v is almost equal to that of one of the horizontal stresses. In a vertical well, the tensile fractures form 180° apart in the direction of S_{Hmax} (Figure 6a). We used the electrical image log to pick drilling-induced tensile fractures along the wellbore from 1900 to 2800 m (6233 to 9186 ft), their presence indicating that, indeed, the stress regime is strike slip to nearly strike slip. An

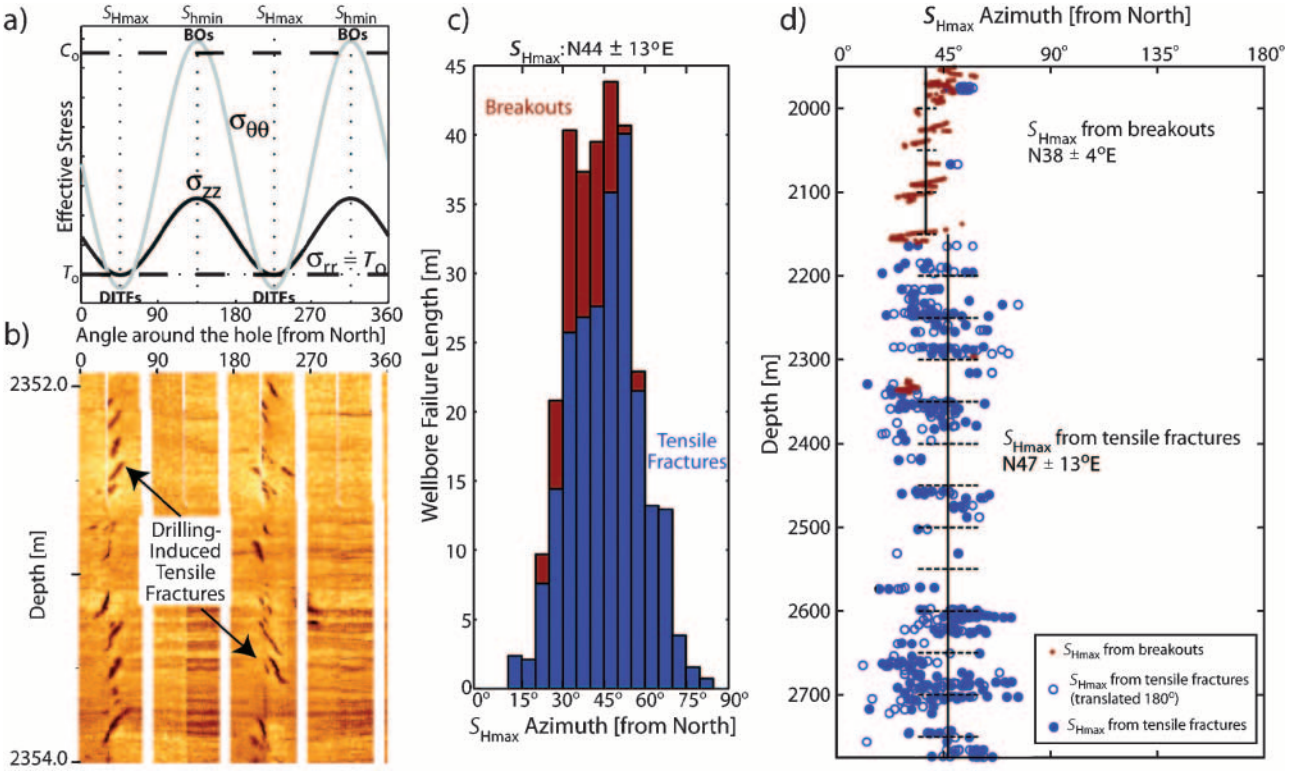

Figure 6. Determining horizontal stress orientation from drilling-induced wellbore failure. (a) Schematic of stress concentrations at the wellbore wall leading to wellbore failure. Where $\sigma_{\theta\theta}$ falls below the tensile strength, T_o, tensile fractures form. Where $\sigma_{\theta\theta}$ is greater than the compressive rock strength, C_o, breakouts form. The orientation of tensile fractures coincides with the far field S_{Hmax} orientation, whereas breakouts form in the direction of S_{hmin}. (b) Example of drilling-induced tensile fractures in the AEP 1 electrical image log. (c) Histogram of S_{Hmax} azimuth where frequency corresponds to length of the wellbore in failure. (d) S_{Hmax} azimuth inferred from tensile fracture and breakout occurrences.

example of drilling-induced tensile fractures from the electrical image log is shown in Figure 6b. The presence of en echelon tensile fractures in the near-vertical wellbore indicates that a small stress perturbation caused the vertical stress to rotate from a principal stress direction (Peska and Zoback, 1995). Based on modeling results, the en echelon fracture pattern observed in the electrical image implies only a small (5–10°) rotation of the vertical stress. As shown below, the state of stress is normal to strike slip in the Rose Run and strike slip in the adjacent formations. This is consistent with the observations of the drilling-induced tensile fractures.

The best data for observing the presence of breakouts are an ultrasonic borehole televiewer (Zoback et al., 1985), but this log was not available for the AEP 1 well. In some instances, breakouts can also be detected in the electrical image as out-of-focus zones, where the pads are not making contact with the wellbore walls. However, the data quality was such that we could not detect breakouts from the electrical image log with certainty. Instead, we used the four-arm caliper data from the electrical image tool to determine the presence of breakouts (Plumb and Hickman, 1985). We analyzed the caliper data for evidence of wellbore elongation. When the difference between the wellbore diameters measured by the two perpendicular caliper arms was greater than 1.02 cm (0.4 in.) and the caliper arms did not rotate more than 15° across a 5-m (16-ft) depth interval, then a breakout was recorded. The hole was considered washed out if the minimum caliper diameter measured more than 1.27 cm (0.5 in.) larger than the drill bit size of 15.5 cm (6.1 in.). The orientation of the caliper pair with the greatest measured diameter determined the azimuth of the breakout and, therefore, the azimuth of S_{hmin}. Because keyseating of the borehole wall can occur from mechanical erosion of the wellbore during the drilling process in wells even slightly deviated from vertical, we checked their occurrence against the direction of the hole to discount this effect.

Taking the breakout and drilling-induced tensile fracture occurrences together, the results of the wellbore failure analysis indicate an average S_{Hmax} orientation

of N44 ± 13°E (Figure 6c). The orientations are corrected for any deviations from vertical in the wellbore trajectory. The breakouts, which occur primarily between 1950 and 2150 m (6397 and 7053 ft), suggest an S_{Hmax} azimuth of N38 ± 4°E (Figure 6d). The drilling-induced tensile fractures occur primarily between 2150 and 2775 m (7053 and 9104 ft), a zone that includes the Rose Run Sandstone, and they indicate an S_{Hmax} azimuth of N47 ± 13°E (Figure 6d). There may be a slight shift in the orientation of S_{Hmax} with depth, or the difference may be an artifact of the less-reliable breakout determinations. Because we have focused on a depth interval in which drilling-induced tensile fractures were observed, we used an S_{Hmax} azimuth of N47 ± 13°E for the geomechanical model of the Rose Run Sandstone and adjacent formations. This S_{Hmax} azimuth is consistent with the regional stress orientations shown with inverted arrows in Figure 1b (Zoback and Zoback, 1989). The presence of borehole failures not only gives the orientation of horizontal stresses, it is also used in conjunction with the other data and observations to constrain the magnitude of S_{Hmax}.

Uniaxial Compressive Strength Measurements

The uniaxial compressive strength, C_o, for four rock samples located in the Rose Run and adjacent dolomite formations was measured in laboratory triaxial tests. Core samples from three different lithologic units indicate very high C_o, particularly in the dolomite layers. The Wells Creek and Beekmantown dolomites have compressive strengths of about 350 MPa. Two samples from the Rose Run Sandstone have C_o values of 238 and 256 MPa. No tests exist for the Queenstone/Reedsville Shale or Trenton Limestone, which are the units with breakouts present. Because breakouts are limited to these units, the rock strength is likely to be significantly less than those determined for the dolomites and sandstone. We estimated a rock strength of 130 ± 25 MPa for these rocks based on observations discussed in the later section on constraining S_{Hmax} magnitudes. Typical C_o values observed for these rock types with similar values for elastic moduli based on the geophysical logs are consistent with this estimation (Chang et al., in press).

Minifrac Test Analysis

The next step in developing a geomechanical model of this site was to measure the magnitude of the least principal stress, S_3, which, in this case, is S_{hmin}. Because drilling-induced tensile fractures already exist along the wellbore wall, when the wellbore fluid pressure exceeds the magnitude of S_{hmin}, a hydraulic fracture should propagate away from the wall in the plane normal to the S_{hmin} direction. The fracture closes when the pressure falls below S_{hmin}. During a minifrac test, a small hydraulic fracture is created, and the pressures at which the fracture forms, propagates, and closes are directly measured. Therefore, minifrac tests are used to determine the magnitude of the least principal stress (Figure 7a). The instantaneous shut-in pressure (ISIP) is a good indicator of the magnitude of S_{hmin}. Once the injection stops, this pressure is reached almost immediately as the fracture closes (Haimson and Fairhurst,

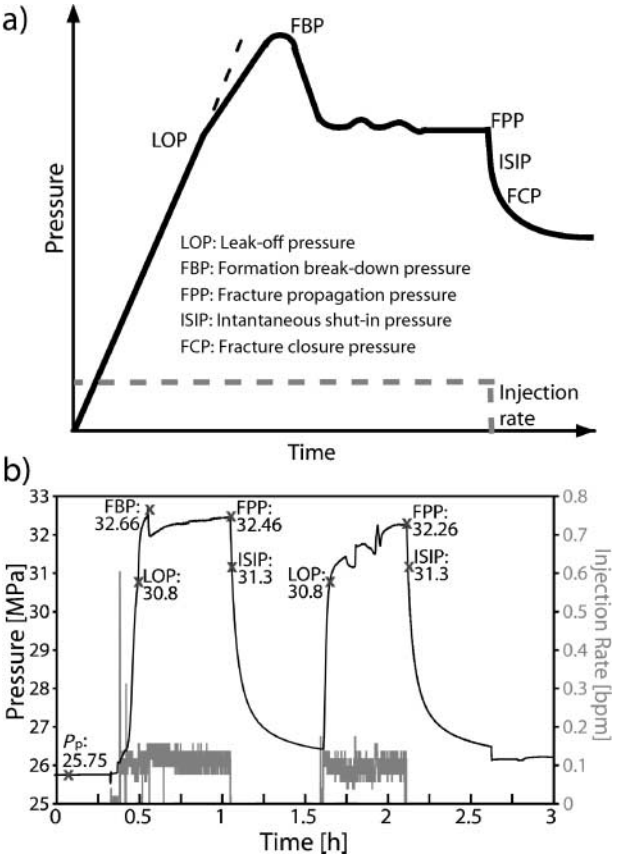

Figure 7. Minifrac tests to measure S_3 magnitude. (a) Example of an ideal minifrac test (Gaarenstroom et al., 1993). Injection rate remains constant until shut-in. Pressure builds linearly until leak-off (LOP) is reached. Pressure declines after the fracture breakdown pressure (FBP). Pressure remains nearly constant at the fracture propagation pressure (FPP) as injection continues. Once injection ends, pressure bleeds off, first reaching the instantaneous shut-in pressure (ISIP) and then the fracture closure pressure (FCP). (b) Minifrac test in the Rose Run Sandstone.

1970). Fracture closure pressure is another common estimate of the least principle stress; however, it is nearly the same as ISIP when low-viscosity fluids and low pumping rates are used during the minifrac. The leak-off pressure and the fracture propagation pressure (FPP) also provide less accurate but reasonable estimates for the least principal stress magnitude when injection rates and fluid viscosities are low.

In AEP 1, five open-hole minifrac tests were completed in and around the Rose Run Sandstone: two tests were completed above it; one test was completed in the sandstone; and two more were completed below it. The tests were conducted using a straddle packer to isolate the test intervals in the uncased borehole section. All the pressure readings for the tests were taken with the same gauge located between the packers. The Rose Run minifrac test was carried out near the top of the unit at 2358.55 m (7738.02 ft) (Figure 7b). We interpreted the S_{hmin} value measured from this test to be 31–32.5 MPa. The results from all the tests and their quality are summarized in Table 1. The tests have varying degrees of quality, the highest being A, which are ranked and explained in the table.

The most notable observation from these results is that the magnitudes of S_{hmin} from the tests in the Rose Run Sandstone and in the rock units directly adjacent to it are significantly lower than the magnitude of S_{hmin} above and below this zone. This difference may be related to the fact that this is a layered system with varying rock stiffness, as illustrated by the variation of log-derived Young's modulus with depth (Figure 4). In a layered system such as this, application of a far-field compressive stress would tend to concentrate stress in the stiffer layers. Correspondingly, stress in the more compliant layers (like the Rose Run Sandstone) would have lower magnitudes than the adjacent layers with greater stiffness. Whereas such a heuristic model is intuitively appealing, it is not possible to accurately match the contrast in stress magnitudes observed with either log-based gravity loading models that predict stress variations with depth based on variations of Poisson's ratio (Anderson et al., 1973; Hareland and Harikrishnan, 1996) or modifications of that model that allow for application of tectonic strain and incorporate variations of Young's modulus with depth (Blanton and Olson, 1999).

The pressure in each test interval was allowed to equilibrate for about 1 day prior to the minifrac tests. The preinjection pressure measurements from the minifrac tests indicate the formation pore pressure (P_p) at depth. We used a linear fit to these data points and obtained a P_p gradient of 11 MPa/km, which is slightly higher than freshwater hydrostatic. This higher gradient is due to the higher density of the high-salinity brine compared to freshwater (Gupta et al., 2005). Given this pressure gradient, the density of CO_2 at the in-situ conditions of the Rose Run Sandstone at 2365 m (7759 ft), with a P_p of 26 MPa and a temperature of 63.1°C, is approximately 782 kg/m^3 (Span and Wagner, 1996).

Constraining S_{Hmax}

To determine the magnitude of S_{Hmax}, we integrated the data and analyses discussed above (rock properties, failure occurrences, stress magnitudes, and pore pressure) along with drilling conditions and the Mohr-Coulomb failure criterion to build constrain stress diagrams as described by Moos and Zoback (1990). The first step was creating a stress polygon that constrains the possible stress relationships between S_{Hmax} and S_{hmin} allowable under the Mohr-Coulomb failure criterion for a given depth. The sides of this polygon are

Table 1. Results of Minifrac Test Analysis*

Depth (m)	Lithologic Unit	S_{hmin} Range (MPa)	Test Quality	Reason for Quality Rating
2077	Trenton Ls.	42→	B	Unclear if FBP or FPP reached
2343	Beekmantown Dol.	35–37	A	Good test
2359	Rose Run Ss.	31–32.5	A	Good test
2413	Copper Ridge Dol.	34→	C	Unclear if FBP or FPP reached; injection rate not constant
2418	Copper Ridge Dol.	44–48	C	Injection rate unavailable; ISIP difficult to pick

*The S_{hmin} magnitude range represents the instantaneous shut-in pressure (ISIP) to the fracture propagation pressure (FPP). In some tests, it is unclear if the pressure increased above the fracture breakdown pressure (FBP) or FPP. These tests are given a lower quality rating. Tests with poor injection rate data quality are ranked the lowest. The S_{hmin} magnitude has a local minimum in the Rose Run Sandstone.

functions of S_v, P_p, and the coefficient of sliding friction (μ) for the specified depth. Laboratory experiments have shown that at depth μ tends to fall within the range of 0.6–1.0 (Byerlee, 1978). In this case, we used the S_v gradient of 26.2 MPa/km, the P_p gradient of 11 MPa/km, and $\mu = 0.8$ to define the dimensions of the polygon (Figure 8). Once the polygon was created, we further constrained the possible state of stress by incorporating the presence or absence of drilling-induced tensile fractures and/or breakouts, along with breakout width if present. Several other inputs are needed to constrain the stress state consistent with the occurrence of wellbore failures at a given depth. These include material properties, drilling conditions, and an estimate of S_{hmin} magnitude. The necessary material properties are Poisson's ratio, ν, Young's modulus, E, the coefficient of thermal expansion, α, and tensile and compressive strengths, T_o and C_o, respectively. Drilling conditions that can influence the formation of drilling-induced wellbore failures are ΔT, the difference between the formation temperature and the mud temperature, and ΔP, the pressure difference between the well pressure (from drilling mud weight) and formation pressure (P_p). In this case, the mud weight is equal to P_p, so $\Delta P = 0$. The final constraint in determining the S_{Hmax} magnitude is the S_{hmin} magnitude obtained (or extrapolated) from the minifrac test results. The values used to build the constrain stress plots are provided in Table 2.

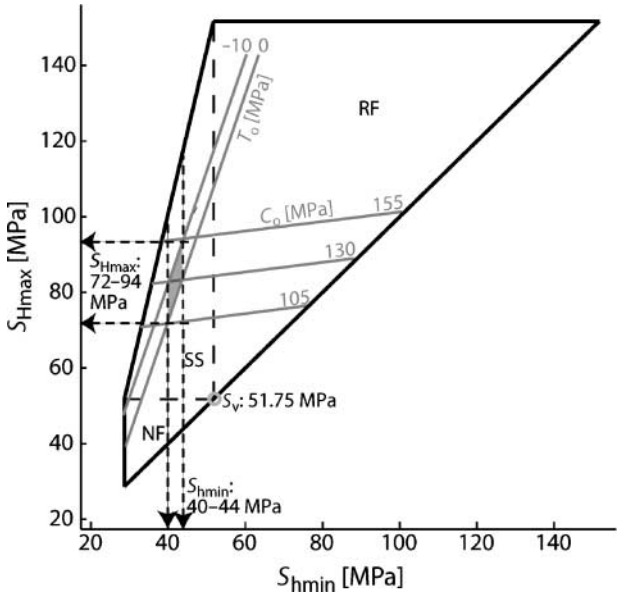

Figure 8. S_{Hmax} magnitude estimation from constrain stress method in Trenton Limestone at a 1975-m (6479-ft) depth. Because breakouts and tensile fractures are observed at this depth, the C_o contours (105, 130, and 155 MPa) and the T_o contours (−10 and 0 MPa) are used to constrain the possible stress magnitudes. Given the S_{hmin} constraint of 40–44 MPa, the gray-shaded region represents the S_{hmin}/S_{Hmax} magnitudes, consistent with all the data and observations at this depth.

Because of the close spacing of most of the minifrac tests, we picked nine depths with wellbore failure observations at which to constrain S_{Hmax} magnitudes (Table 2). First, we examined the stress state in the cap rock. We show in Figure 8 one example of using the constrain stress diagram to estimate the magnitude of S_{Hmax} at a depth of 1975 m (6479 ft). The black polygon outlines the possible stress magnitudes constrained by frictional rock strength and Mohr-Coulomb failure criteria. The presence of both drilling-induced tensile fractures and breakouts at this depth provides further constraints on the stresses. The −10- and 0-MPa contours reflect the range in tensile strength, T_o, assumed for the rock. Because tensile fractures are observed, the stresses must fall between the contours. If no tensile fractures were observed, then the stresses would fall to the right of the contours. The 105-, 130-, and 155-MPa contours represent different C_o values. Because breakouts are observed, the stresses are constrained to lie between the C_o contours corresponding to the estimated C_o magnitude range of the rock. If breakouts were not observed, then the stresses would lie below the C_o contour for the estimated rock strength. However, because no rock strength measurements were made in this formation, this constraint is not used in this particular case. Instead, the S_{hmin} magnitudes determined from the minifrac tests act as the final constraint for isolating allowable S_{hmin}/S_{Hmax} relationships. We used S_{hmin} magnitudes ranging between a lower bound of 40 MPa and an upper bound of 44 MPa to constrain S_{Hmax}. We used this range because the closest minifrac test was taken at 2076.9 m (6813.9 ft) and has uncertainty associated with it (Table 1). Based on the S_{hmin}, tensile fracture, and breakout constraints, we can estimate that the rock strength in the Trenton Limestone is 130 ± 25 MPa. This rock strength estimate is likely to be applicable to other formations where breakouts are present. Therefore, we used C_o equal to 130 ± 25 MPa as an additional constraint in stress determinations where breakouts were present, but drilling-induced tensile fractures were not. From this information, we estimate an S_{Hmax} magnitude of 83 ± 11 MPa (Table 3). The possible range in S_{hmin} and S_{Hmax} values in the Trenton Limestone at 1975 m (6479 ft) is highlighted by the shaded region in Figure 8. At this depth, S_v is the intermediate principal stress, such that the

Table 2. Input Data and S_{hmin} Constraints for the S_{Hmax} Constrain Stress Determinations*

Depth (m)	S_v (MPa)	P_p (MPa)	Wellbore Failure Type	B_0 Width (°)	Poisson's Ratio	Young's Modulus (GPa)	C_o (MPa)	ΔT (°C)	S_{hmin} (MPa)
1925	50.44	21.18	BO	50	0.29	60	105–155	−7	40–44
1975	51.75	21.73	BO, DITF	50	0.31	74	105–155	−7.8	40–44
2050	53.71	22.55	BO	50	0.31	76	105–155	−9	41–45
2125	55.67	23.38	BO	50	0.3	68	105–155	−10.25	42–46
2265	59.34	24.92	DITF	0	0.29	94	350	−12.5	44–48
2365	61.96	26.02	DITF	0	0.25	85	240	−14.1	34–36
2465	64.58	27.12	DITF	0	0.28	95	350	−15.7	46–50
2502	65.55	27.52	DITF	0	0.28	100	350	−16.3	47–51
2625	68.77	28.88	DITF	0	0.27	72	350	−17.8	49–53

*The S_v gradient is 26.2 MPa/km. The P_p gradient is 11 MPa/km. Wellbore failure types are drilling-induced tensile fractures (DITF) and breakouts (BO). Breakouts are assumed to have a width of 50°. Poisson's ratio and Young's modulus values come from the geophysical logs (Figure 4) and are used to approximate the static moduli. Compressive rock strength, C_o, for the four shallowest depths are from the results of the constrain stress diagram at 1975 m (6479 ft) (Figure 8). The other C_o values are from the triaxial test results. The value of ΔT is the temperature difference of the drilling fluids and the formation temperature. The S_{hmin} constraints are based on the minifrac test analysis. Inputs that remained constant for all depths are a coefficient of thermal expansion of 5.4×10^{-6}/°C, and ΔP equals zero.

stress state in the Trenton Limestone falls within the strike-slip stress regime.

In the Rose Run Sandstone, we constrained the stress at 2365 m (7759 ft). This is slightly deeper than the minifrac test depth (2358 m; 7736 ft). We used a range for S_{hmin} of 34–36 MPa because of the low values of S_{hmin} suggested by the minifrac tests at 2343, 2358, and 2413 m (7687, 7736, and 7916 ft) (Table 1). The S_{hmin} lower bound of 34 MPa at this depth is constrained by the Mohr-Coulomb failure criterion for normal faulting. Based on the S_{hmin} constraint and the presence of drilling-induced tensile fractures, we interpreted the S_{Hmax} magnitude to be 52.5 ± 10.5 MPa, falling in the normal faulting to strike-slip stress regime (S_v is the greatest principal stress). The S_{Hmax} determinations for all the depths are shown in Figure 9 and outlined in Table 3, along with P_p, S_v, minifrac interpretation results, and approximate S_{hmin} used to constrain the S_{Hmax} magnitudes.

Results and Implications of the Geomechanical Analysis

To briefly summarize, using several types of data and observations, we were able to constrain the in-situ state of stress at the Mountaineer site. We calculated S_v to

Table 3. Results of the Maximum Horizontal Stress Magnitude Analysis*

Lithologic Unit	Depth [m]	P_p [MPa]	S_{hmin} [MPa]	S_v [MPa]	S_{Hmax} [MPa]
Queenstone Sh.	1925	21.2	40–44	50.4	71–88
Trenton Ls.	1975	21.7	40–44	51.7	72–94
Trenton Ls.	2050	22.5	41–45	53.7	73–90
Trenton Ls.	2125	23.4	42–46	55.7	74–91
Trenton Ls.	2265	24.9	44–48	59.3	75–95
Top Rose Run Ss.	**2355**	**25.9**	**31–32****	**61.7**	**42–63**
Rose Run Ss.	2365	26.0	34–36	62.0	42–63
Bottom Rose Run Ss.	**2388**	**26.3**	**35–37**	**62.6**	**42–63**
Copper Ridge Dol.	2465	27.1	46–50	64.6	73–95
Copper Ridge Dol.	2502	27.5	47–51	65.5	73–95
Nolichucky Sh.	2625	28.9	49–53	68.8	81–100

*Using the constrain stress method along with the other principal stress magnitudes and pore pressures. Included in bold for reference at each depth are estimates of stress magnitudes and pore pressure at the top and bottom of the Rose Run Sandstone.

**Indicates that the value is from a minifrac test.

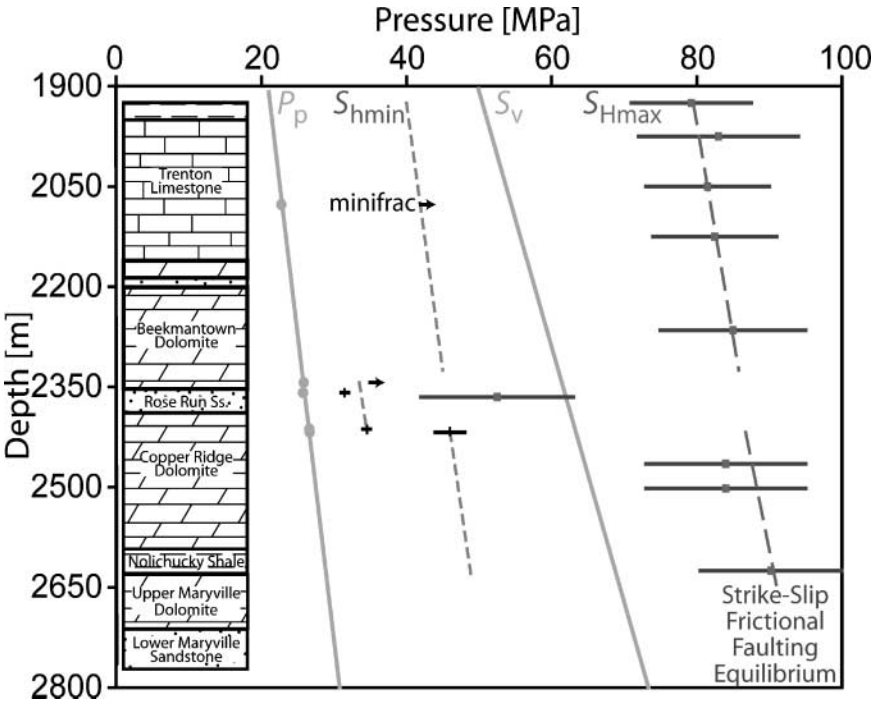

Figure 9. Pressure-versus-depth plot of the stress magnitude results. The P_p gradient determined from minifrac test data is 11 MPa/km. The S_v gradient is 26.2 MPa/km. The minifrac test analysis (black) indicates that the S_{hmin} magnitude has two trends, illustrated by the gray dashed lines (short dashes). The S_{hmin} magnitude in and around the Rose Run Sandstone is significantly less than that above and below this zone. The S_{Hmax} estimates from the constrain stress method are shown with solid gray bars. The dashed gray line (long dashes) is the S_{Hmax} value predicted by frictional faulting theory for a strike-slip stress regime based on the measured values of S_{hmin} and P_p and a coefficient of sliding friction of 0.6.

have a gradient of 26.2 MPa/km. The electrical image log and caliper data allowed us to establish the horizontal stress orientations in the Rose Run Sandstone and adjacent dolomites, with S_{Hmax} oriented N47°E (±13°) and S_{hmin} oriented N43°W (±13°). The minifrac test analysis provides the magnitude for the least principal stress, which, at this site, is S_{hmin}, for specific depths. The minifrac data show a significant difference in S_{hmin} magnitude between the Rose Run Sandstone and adjacent formations, which may be a function of the variability of the rock stiffness. The P_p in the formations, as measured during the minifrac testing, is nearly hydrostatic with a gradient of 11 MPa/km. Through the integration of stress and P_p data with calculated rock properties and information about the drilling operations, we constrained the magnitude of S_{Hmax} with depth (Figure 9; Table 3).

The state of stress in the cap rock is in a strike-slip stress regime, where $S_{hmin} \leq S_v \leq S_{Hmax}$. The Rose Run Sandstone appears to be in a normal faulting regime, where S_{Hmax} is the intermediate principal stress. This stress variation with depth is beneficial in terms of the CO_2 sequestration potential of the Rose Run Sandstone. Because of the much lower value of the least principal stress in and around the Rose Run Sandstone relative to that of the surrounding formations, this layer will allow for hydraulic fracture propagation at much lower pressures than the formations above and below. Therefore, it would be possible to fracture this zone during injection without compromising the integrity of the cap rock. The benefits of hydraulic fracturing for increasing injectivity are investigated in the next section of this paper using geostatistical aquifer modeling and fluid-flow simulations. Also, the wellbore wall stability of deviated wells is examined for both the cap rock and Rose Run Sandstone stress states.

Furthermore, the stress state of the cap rock appears to be in strike-slip faulting frictional equilibrium (Figure 9). That is, the stress magnitudes are limited by the frictional strength of widely distributed, preexisting planar discontinuities in the crust as reviewed by Townend and Zoback (2000) and discussed by many others. Therefore, perturbations in the state of stress, such as pore-pressure changes caused by fluid injection, may induce shear slip if optimally oriented faults are present and the pressure perturbations are large enough. To investigate the possibility of inducing seismicity, we need to determine which faults are optimally oriented in the in situ stress state and what increase in pore pressure would result in slip on those faults.

It should be noted that a coupling between stress magnitudes and pore pressure exists such that the increases in pore pressure associated with CO_2 injection are expected to lead to increases in the horizontal stress magnitudes. The extent of this effect can be predicted using the poroelastic theory. As discussed by Brown et al. (1994), assuming no lateral strain, the change in

total horizontal stress (ΔS_{hor}) for a given change in pore fluid pressures (ΔP_p) can be determined by

$$\Delta S_{hor} = \alpha \Delta P_p \left(\frac{1 - 2\nu}{1 - \nu} \right) \quad (7)$$

where ν is Poisson's ratio, and α is Biot's coefficient ($\alpha = 1 - K_b/K_g$, where K_b is the bulk modulus of the dry rock, and K_g is the bulk modulus of the rock-forming mineral). At the Mountaineer site, the mean ν is 0.28, and α ranges from 0.03 to 0.2, with a mean of 0.1. For the mean case, the ΔS_{hor} would be about $0.06\Delta P_p$. Because the effect of the pressure change on stress magnitude is so small, it is not considered in the following work.

MODELING AND SIMULATION OF CO_2 INJECTION

Several tools and techniques commonly applied in the petroleum industry are valuable for assessing the CO_2 sequestration potential in deep saline reservoirs. Modeling 3-D reservoir geometry and stochastic simulation of petrophysical properties are important techniques for capturing the geological characteristics and heterogeneities of potential CO_2 injection sites while accounting for different levels of uncertainty. These models are then used as inputs into fluid-flow simulations. Numerical flow simulations using robust 3-D reservoir models provide estimates of fluid-flow behavior, fluid interactions, and sequestration capacity in deep saline formations, even when there are limited data available. Furthermore, as we have mentioned, reservoir-stimulation techniques, such as hydraulic fracturing, may be needed to improve injectivity in the less porous and less permeable deep aquifers. The benefits of reservoir stimulation can be evaluated with the aid of appropriate reservoir models and flow simulation analysis. Fluid-flow simulation studies are an integral step in understanding and quantifying CO_2 sequestration potential not only in deep aquifers but also in other geological settings.

Modeling Reservoir Architecture

Given the information collected during the Mountaineer site characterization, we built two 3-D reservoir models to represent the Rose Run Sandstone. It should be noted that more detailed compositional reservoir modeling to develop injection and monitoring system designs is being conducted separately (White et al., 2005), and that the current simulations are specifically focused on the geomechanical aspects. Two models were used in this study to represent the Rose Run Sandstone: (1) in its native state and (2) with a stimulated hydraulic fracture. The geometry of the models is the same and was based on a regional data set for the Rose Run Sandstone, which indicates a N10°E strike, a gentle 2–3° dip to the southeast, and a thickness varying on average between 15 and 50 m (49 and 164 ft). At the Mountaineer site, the top of the Rose Run is at 2355-m (7726-ft) depth, and the unit is 33 m (108 ft) thick (from AEP 1 well data). We built a 6 × 6-km (3.7 × 3.7-mi) grid centered around the AEP 1 well. To introduce a hydraulic fracture, we oriented the grid blocks in a direction consistent with that of S_{Hmax}, N45°E (Figure 6c, d). The width of the grid blocks along the center diagonal is about 1 m (3.3 ft) in the northwest-southeast direction, to approximate the presence of a hydraulic fracture. We determined that a 150 × 172 × 5 grid allowed for efficient simulation runs while maintaining a significant amount of information on the aquifer properties. We used the same grid for both models, but populated the petrophysical properties differently.

We used the sequential Gaussian simulation (SGS) method (Isaaks, 1990) to produce equally probable realizations of porosity and permeability that reflect the data variability and spatial statistics while incorporating both hard (i.e., well data) and soft (i.e., property correlations) data (Deutsch, 2002). The only hard data available on permeability and porosity for the location came from the NMR permeability and density-porosity logs of the AEP 1 well (Figure 3). Based on these porosity and permeability data, we chose consistent, yet subjective, distributions to use in the property simulations of the larger scaled grid (Figure 10). We investigated a lower and upper bound of permeability with the distributions differing by an order of magnitude to reflect the uncertainty in the upscaled permeability values. By plotting the density-porosity log data against the NMR permeability data (log scale), we found a correlation coefficient of 0.65, which we used as soft data in the property simulations. The spatial variability of the properties was incorporated into the SGS algorithm using a semivariogram. Because of the lack of data, our choice of semivariogram was highly subjective. Because the Rose Run Sandstone is in a sedimentary basin, we expect a significant amount of lateral correlation in the properties. We chose a normalized, spherical semivariogram model with a 0.2 nugget effect and an isotropic range of 500 m (1600 ft) in the geological coordinate

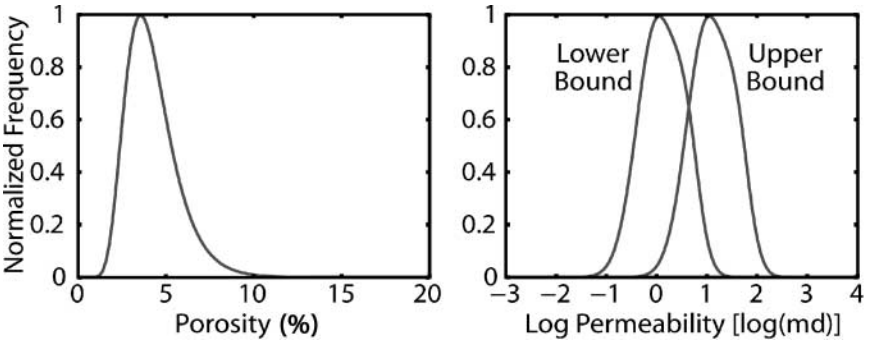

Figure 10. Porosity and log permeability histograms used in the sequential Gaussian simulation algorithm to populate the aquifer models with petrophysical properties. Porosity is modeled with a lognormal distribution; log permeability is modeled with a multi-Gaussian distribution. The lower and upper bound permeabilities differ by an order of magnitude.

system. We created 20 realizations: five realizations for each of the permeability distributions for both of the models (without and with a hydraulic fracture). To incorporate the hydraulic fracture in the second model, we assigned a porosity of approximately 30% and permeability of 1000 md to the thin grid blocks extending 300 m (1000 ft) from the center grid block (AEP 1 well location) along the N45°E axis. We believe that these property values approximate those associated with the fracture and surrounding formation after fracturing.

CO_2 Injection Simulations

We used a commercial black-oil simulator for these preliminary flow simulations. Whereas the simulator has limitations when simulating CO_2 injection, it has sufficient capabilities for the purpose of this study. Namely, we were looking for the approximate magnitude of CO_2 injection throughout 30 yr, the effect that a hydraulic fracture with a 300-m (1000-ft) half-length would have on injection rate, and the changes in reservoir pore pressure with injection. The simulator input is based on the characterization and geomechanical analysis of the Mountaineer site. The temperature of the Rose Run Sandstone is 63°C. The pore-pressure gradient is 11 MPa/km. The injection rate of the AEP 1 well is controlled by a bottom-hole pressure (BHP) constraint. In the case with no hydraulic fracture, the BHP constraint is set at 32 MPa, which is close to the fracture pressure of the Rose Run Sandstone as determined in the geomechanical analysis. The BHP constraint in the hydraulically fractured case is 42 MPa, which is just below the fracture pressure of the cap rock. We included producer wells along the boundary of the grid to enforce a constant pressure boundary condition that is consistent with the open system of the reservoir. These wells produce when their BHP exceeds the ambient 11 MPa/km gradient. In the simulator, water was modeled as oil and CO_2 as gas, allowing the CO_2 to dissolve in the water. The fluid properties of the water and CO_2 are functions of pressure and temperature and salinity in the case of water. On average, the values are water formation factor (Bw) of 1.04 reservoir m^3/standard m^3, CO_2 formation factor of 1.8×10^{-3} reservoir m^3/standard m^3, water viscosity of 7.3×10^{-4} Pa·s (0.73 cp), and CO_2 viscosity of 1.01×10^{-4} Pa·s (0.101 cp). The CO_2 solubility is dependent on temperature, pressure, and salinity, the effects of which are modeled by a Sechnow coefficient and fitted to literature data (J. Ennis-King, 2004, personal communication). The CO_2 solubility (Rsw) calculated at reservoir temperature and salinity ranged from 29.7 to 33.9 standard m^3/standard m^3 over pressures of 25–42 MPa. We used relative permeability curves adapted from the van Genuchten (1980) function with an irreducible gas saturation of 0.05, an irreducible liquid saturation of 0.2, and an exponent (λ) of 0.457, resulting in crossover at 0.75 gas saturation. Variations of the van Genuchten relative permeability function were implemented in several test problems in the Pruess et al. (2002) numerical simulation code comparison study. By using a small residual gas saturation, we can account for the presence of isolated gas. This could occur because of snap-off mechanisms that act when the pore body-to-pore throat ratio is large, or when dissolved CO_2 comes out of solution in isolated low pressure areas.

We simulated CO_2 injection for 30 yr on all 20 realizations. The CO_2 saturation and formation pressure are shown in Figure 11 for one realization of each model for both permeability distributions. In all cases, as expected, the pressure front moves out ahead of the CO_2 front, with the highest reservoir pressures closest to the well (Figure 11). This is consistent with the values of the fluids' compressibilities. The hydraulic fracture increases injection rate and cumulative injection by nearly a factor of four over the nonfractured cases (Figure 12). In the lower bound permeability realizations, the injection rate remains nearly constant after 5 yr, at about 8 kt CO_2/yr (without fracture) and 31 kt CO_2/yr (with fracture). A small amount of variability is apparent

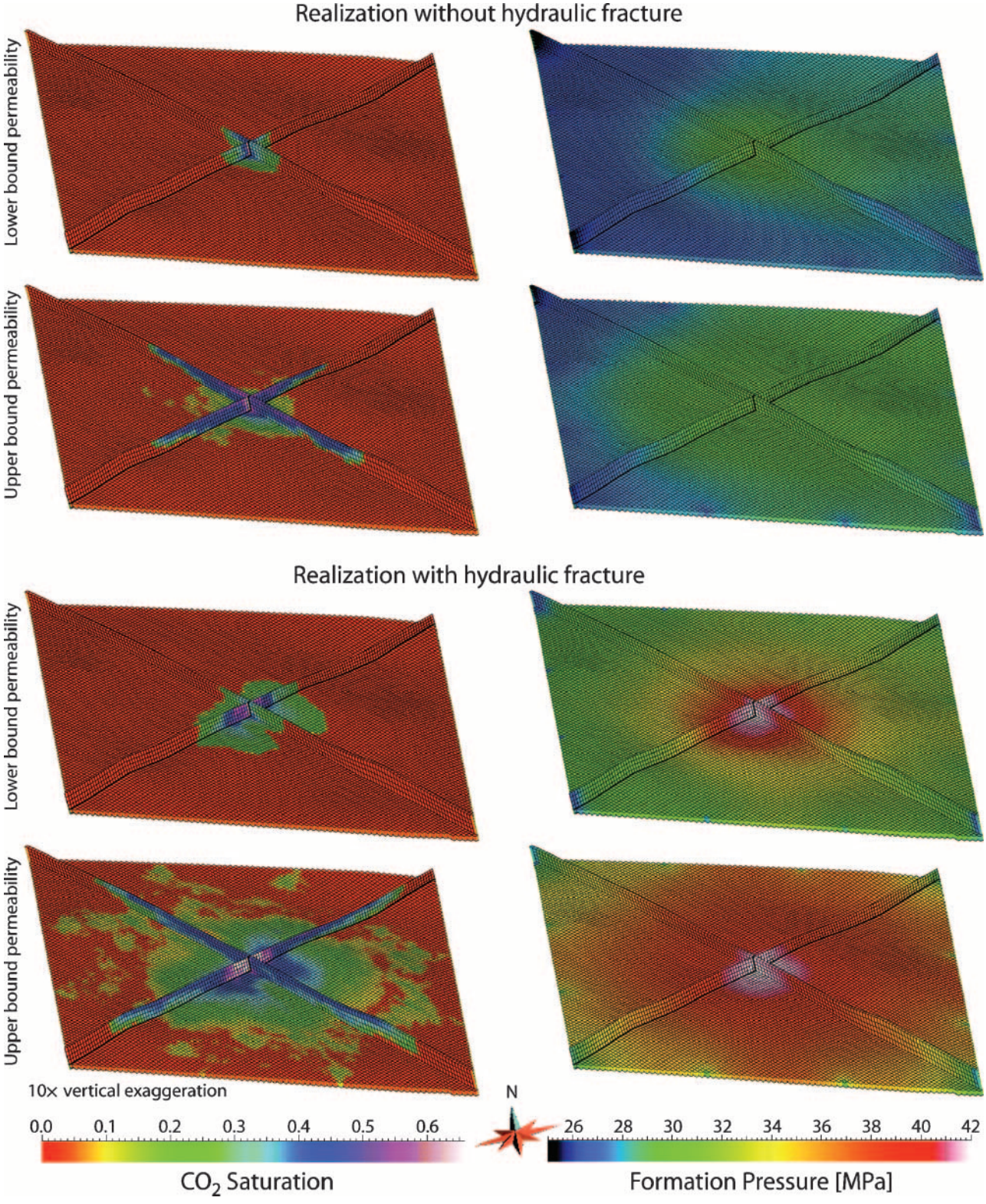

Figure 11. CO_2 injection simulation results after 30 yr for the lower and upper bound permeability fields for one realization of each of the two models. The lateral extent of the grid is 6 × 6 km (3.7 × 3.7 mi). The presence of the hydraulic fracture significantly increases total amount of CO_2 injected. To prevent a fracture from forming in the realization without a hydraulic fracture, the bottom-hole pressure (BHP) constraint must be below the fracture pressure of the injection zone. In the fractured case, the injection rate is controlled by a higher BHP constraint, which is just below the cap-rock fracture pressure. Therefore, the total aquifer pressure is much higher in the fractured simulations.

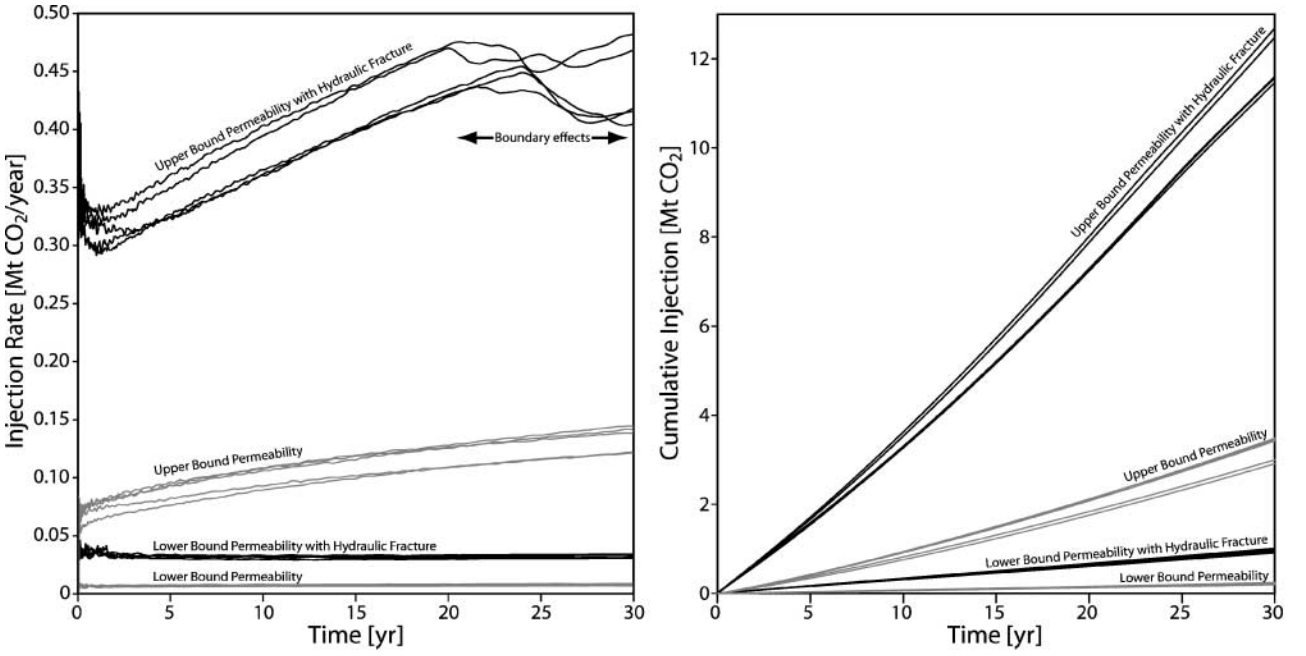

Figure 12. CO_2 injection rate and cumulative CO_2 injection throughout 30 yr for 20 realizations.

between realizations. In the upper bound permeability cases, the effects of relative permeability can be observed. As the CO_2 saturation increases near the injection well, the CO_2 flows more easily, resulting in an increased injection rate with time. In these simulations, the injection rate increases with time, from about 70 to 140 kt CO_2/yr (without fracture) and from about 320 to 470 kt CO_2/yr (with fracture). In the upper bound permeability realizations, the cumulative injection after 30 yr is 12–15 times higher than that of the associated lower bound permeability realizations. Further increase in the injection rates at the site may be possible with the use of the horizontal or multilateral wells and multiple injection zones. In the fractured model-upper bound permeability cases, the CO_2 reaches the extent of the 6 × 6-km (3.7 × 3.7-mi) area (Figure 11). We also observed that the injection rate in these cases is affected by the grid boundaries after injecting about 10 Mt CO_2 (Figure 12). These results suggest that every 10–12 Mt of CO_2 injected requires about a 6 × 6-km (3.7 × 3.7-mi) area given the thickness and porosity of the Rose Run Sandstone.

HORIZONTAL WELL STABILITY

Another option for increasing CO_2 injection is drilling horizontal wells that extend several hundred meters in the injection zone. These wells would remain uncased to maximize the surface area through which the CO_2 could enter the formation. Because the horizontal wells remain open and deviated drilling tends to be more difficult than vertical drilling, we examined which orientations would be favorable for deviated wells to remain stable in the local stress field. To evaluate well stability, we determined the necessary rock strength, C_o, needed to completely prevent breakouts from occurring for various well orientations given the stress state determined in the geomechanical analysis. For simplicity, the analysis assumes balanced drilling, in which the mud weight equals the formation pore pressure. This is an extremely conservative analysis because, in many cases, a well will remain stable even with breakouts present and breakout widths up to 70–90° (39–50% of wellbore wall).

We investigated the stability of wells drilled with varying degrees of deviation from vertical. One case we examine is drilling a horizontal well in the direction of S_{Hmax}, the same direction that a hydraulic fracture would form. In this case, it would be possible to implement both a longitudinal hydraulic fracture along with the horizontal well to increase injectivity if deemed safe and economical. We examined well stability in both the strike-slip stress state of the cap rock and the normal faulting stress state of the injection zone. In this way, we know if the well deviation can begin in the cap rock and continue into the injection unit despite the difference in stress state.

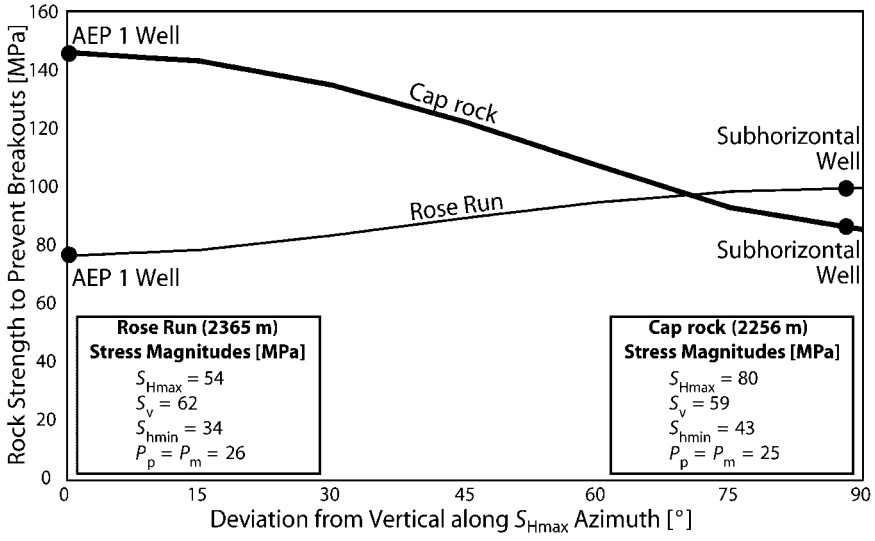

Figure 13. Plot of the change in the minimum required rock strength to prevent breakouts as the well trajectory deviates from vertical in the S_{Hmax} direction. In the cap rock, a well becomes more stable as the borehole deviation increases toward horizontal. In the Rose Run Sandstone, the borehole stability slightly decreases with increased deviation, but the required rock strength to prevent breakouts is still less than that needed for most deviation angles in the cap rock.

The results of this analysis are presented in Figure 13. In the cap rock, we find that, as the well deviation in the S_{Hmax} direction increases from vertical to horizontal, the well stabilizes. In fact, a vertical well like AEP 1 has the least stable well trajectory for the strike-slip state of stress. However, we observed very few breakouts in the cap rock below 2180 m (7152 ft) in this well. In the cap rock stress state, breakouts would form in a northeast-southeast–oriented horizontal well only in rocks with a C_o less than 85 MPa. The measured C_o in the Beekmantown Dolomite is more than 300 MPa; therefore, a deviated well will remain stable in this unit. In the Rose Run Sandstone state of stress, a horizontal well would require a higher C_o to prevent breakouts than a vertical well, so it would be less stable. A horizontal well in the direction of S_{Hmax} has the least stable well trajectory in the injection zone stress state. However, breakouts will only occur in a northeast-southwest–oriented horizontal well in rocks with C_o less than 100 MPa. The C_o measured in the Rose Run Sandstone is more than 200 MPa. Based on this analysis, it is clear that directional drilling can be effectively implemented at the Mountaineer site. Furthermore, the injection process, which is analogous to overbalanced drilling, will continue to support the horizontal well stability.

INVESTIGATING INDUCED SEISMICITY

Injection-induced seismicity occurs when the increase in pore pressure caused by fluid injection decreases the effective normal stress resolved on optimally oriented, preexisting faults such that it induces fault slip. The occurrence of injection-induced seismicity is well documented at several sites in tectonically stable intraplate areas (Pine et al., 1983; Raleigh et al., 1976; Zoback and Harjes, 1997). As previously stated, in a stress state in frictional equilibrium, even small pressure perturbations can induce slip if faults with optimal orientation are present. It is thought that much of the intraplate continental crust is likely in frictional equilibrium (Townend and Zoback, 2000). For this reason, the investigation of induced seismicity potential as it relates to CO_2 sequestration is important for understanding the risks associated with such an endeavor (Sminchak and Gupta, 2003). Although injection-induced seismicity has not been an issue in the past for the Appalachian basin, previous injection has not been at the same scale as CO_2 sequestration, making this an important issue to consider in future site studies. The S_{Hmax} values determined at the Mountaineer site are consistent with the S_{Hmax} magnitudes predicted by Coulomb frictional-failure theory, assuming that the coefficient of friction on preexisting faults is 0.6 (Figure 9). The frictional equilibrium stress state is also supported by the drilling-induced tensile fractures observed along much of the borehole from 2150 to 2775 m (7053 to 9104 ft).

Figure 14a illustrates the fault orientations and associated changes in the pore pressure, P_p, that could lead to induced seismicity near the Mountaineer site. Hot colors indicate that small increases in P_p could result in slip. The black dots are fracture pole orientations of fractures observed in the Beekmantown Dolomite on the electrical image log. The white dots are the fracture poles of hypothetical optimally oriented faults. They represent the orientations of the faults that are most likely to slip given the in-situ stress state in the cap rock. Assuming that the coefficient of sliding friction along

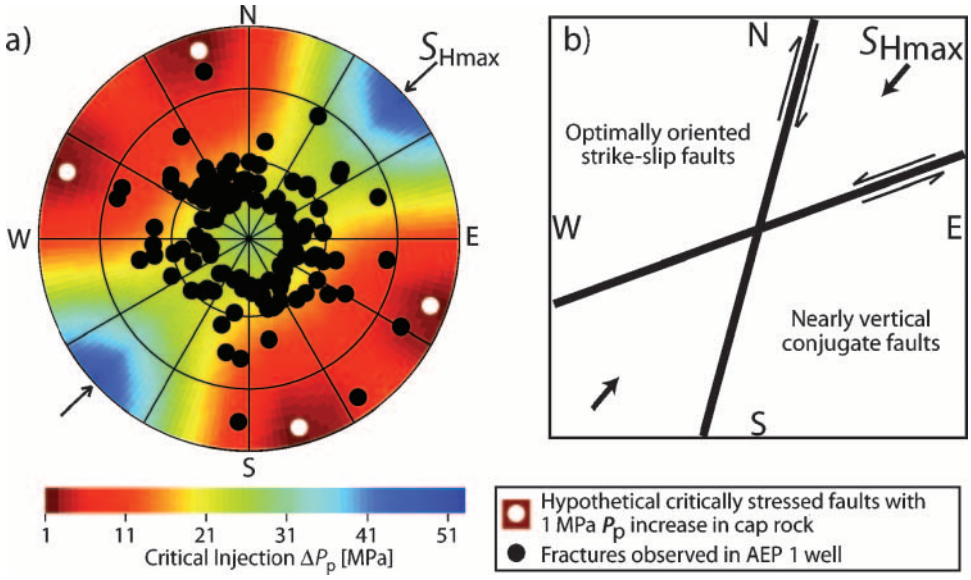

Figure 14. Induced seismicity and critically stressed faults in the cap rock. (a) Lower hemisphere stereonet plot of critical pore pressure changes because of injection as a function of fracture pole-to-plane orientation. Each location in the circle represents a pole perpendicular to a fracture plane projected onto a two-dimensional representation of the lower half of a sphere. The colored bar indicates the amount that the P_p would need to increase above the initial state to induce slip on existing faults with a certain fracture pole orientation. Areas with hot colors represent fracture pole orientations that are likely to slip with small P_p perturbations. The black circles are fracture poles of fractures observed in the AEP 1 electrical image log of the Beekmantown Dolomite from 2200 to 2350 m (7217 to 7709 ft). The white circles are the hypothetical fracture poles that would be most likely to slip given a small P_p increase in the current state of stress. (b) Map view schematic of faults corresponding to the hypothetical fracture pole orientations shown in white on the stereonet plot.

the optimal fault planes is 0.6, reactivation could occur with very small increases in P_p. The optimally oriented faults for the cap rock stress state are nearly vertical strike-slip faults that strike north-northeast or east-northeast (Figure 14b). If the coefficient of sliding friction along the faults is higher (e.g., 0.8), a larger P_p perturbation is necessary to induce slip. Likewise, faults with less optimal orientations require greater P_p changes for slip to occur. The results suggest that further work on the topic is necessary to understand the risks of sequestering CO_2 in the Appalachian Basin. Given that small P_p perturbations have the potential to induce seismicity in the given stress state, and the lack of laterally extensive data for identifying faults in the area, monitoring of microseismic events will be an important technique for any sequestration project in the region.

CONCLUSIONS

The limited thickness and low to moderate porosity and permeability of the Rose Run Sandstone are formidable challenges to the injection and sequestration of the CO_2 emitted from the Mountaineer power plant. Similar challenges may hamper sequestration in other deep aquifer settings in the region. At the Mountaineer site, the dominant stress state is strike-slip faulting near frictional equilibrium. However, the stress state in the Rose Run Sandstone is normal faulting. The lower magnitude of S_{hmin} in the Rose Run Sandstone (compared to adjacent units) makes it attractive to use hydraulic fracturing to stimulate injectivity. A 300-m (1000-ft) half-length hydraulic fracture increases injectivity by nearly a factor of 4. If the average formation permeability is more similar to an assumed upper-bound distribution (2–63 md), the preliminary simulations indicate a maximum injection of about 6% of the Mountaineer emissions (7 Mt/yr) for a single vertical well with an induced hydraulic fracture in the Rose Run Sandstone injection zone. Assuming a 30-m (100-ft) average thickness and a porosity ranging between 2 and 10%, up to a 600-km^2 (231-mi) area may be needed to accommodate the volume of CO_2 from the Mountaineer plant to be injected throughout 30 yr (about 210 Mt). This likely requires sequestration in multiple horizons and the use of hydraulic fractures and/or extended horizontal injection wells. Induced seismicity in the cap rock could occur with small increases in P_p if optimally

oriented faults are present. As the pressure front associated with injection moves ahead of the CO_2 front, if induced seismicity occurred, injection could be terminated prior to the CO_2 front reaching the fault(s) associated with the induced seismicity, thus limiting the risk of leakage. These conclusions suggest that microseismic networks should be part of CO_2 sequestration monitoring programs in the region.

REFERENCES CITED

Anderson, R. A., D. S. Ingram, and A. M. Zanier, 1973, Determining fracture pressure-gradients from well logs: Journal of Petroleum Technology, v. 25, p. 1259–1268.

Blanton, T. L., and J. E. Olson, 1999, Stress magnitudes from logs: Effects of tectonic strains and temperature: Society of Petroleum Engineers Reservoir Evaluation and Engineering, v. 2, p. 62–68.

Brown, K. M., B. Bekins, B. Clennell, D. Dewhurst, and G. K. Westbrook, 1994, Heterogeneous hydrofracture development and accretionary fault dynamics: Geology, v. 22, p. 259–262.

Byerlee, J., 1978, Friction of rocks: Pure and Applied Geophysics, v. 116, p. 615–626.

Chang, C., M. D. Zoback, and A. Khaksar, in press, Rock strength and physical property measurements in sedimentary rocks: Journal of Petroleum Science and Engineering.

Deutsch, C. V., 2002, Geostatistical reservoir modeling: New York, Oxford University Press, 376 p.

EPA, 2002, Egrid2002: Emissions and generation resource integrated database, Volume 2.01: http://www.epa.gov/cleanenergy/egrid/download.htm (accessed November 15, 2004).

Gaarenstroom, L., R. A. J. Tromp, M. C. Jong, and A. M. Brandenburg, 1993, Overpressures in the central North Sea: Implications for trap integrity and drilling safety, *in* J. R. Parker, ed., Petroleum geology of northwest Europe: 4th Conference, p. 1305–1313.

Gupta, N., P. Jagucki, D. Meggyesy, F. Spane, T. S. Ramakrishnan, and A. Boyd, 2005, Determining carbon sequestration reservoir potential at a site-specific location within the Ohio River Valley region, *in* E. S. Rubin, D. W. Keith, and C. F. Gilboy, eds., Proceedings of the 7th International Greenhouse Gas Control Technologies (GHGT-7), v. 1: Vancouver, Canada, Elsevier, p. 511–520.

Haimson, B., and C. Fairhurst, 1970, In situ stress determination at great depth by means of hydraulic fracturing, *in* W. H. Somerton, ed., 11th Symposium on Rock Mechanics: London, Society of Mining Engineers of the American Institute of Mining Metallurgical and Petroleum Engineers, p. 559–584.

Hareland, G., and R. Harikrishnan, 1996, Comparison and verification of electric-log-derived rock stresses and rock stresses determined from the Mohr failure envelope: Society of Petroleum Engineers Formation Evaluation, v. 11, p. 219–222.

Isaaks, E. H., 1990, The application of Monte Carlo methods to the analysis of spatially correlated data: Ph.D. thesis, Stanford University, Stanford, California, 213 p.

Jaeger, J. C., and N. G. W. Cook, 1979, Fundamentals of rock mechanics: London, Chapman and Hall, 593 p.

Kirsch, G., 1898, Die theorie der elastizitat und die bedurfnisse der festigkeitslehre: Zeitschrift des Vereines Deutscher Ingeniere, v. 42, p. 797–807.

Moos, D., and M. D. Zoback, 1990, Utilization of observations of well bore failure to constrain the orientation and magnitude of crustal stresses— Application to continental, Deep-Sea Drilling Project, and Ocean Drilling Program boreholes: Journal of Geophysical Research— Solid Earth and Planets, v. 95, p. 9305–9325.

Peska, P., and M. D. Zoback, 1995, Compressive and tensile failure of inclined well bores and determination of in-situ stress and rock strength: Journal of Geophysical Research— Solid Earth, v. 100, p. 12,791–12,811.

Pine, R. J., P. Ledingham, and C. M. Merrifield, 1983, In situ stress measurement in the Carnmenellis Granite: II. Hydrofracture tests at Rosemanowes Quarry to depths of 2000 m: International Journal of Rock Mechanics and Mining Sciences, v. 20, p. 63–72.

Plumb, R. A., and S. H. Hickman, 1985, Stress-induced borehole elongation— A comparison between the 4-arm dipmeter and the borehole televiewer in the Auburn geothermal well: Journal of Geophysical Research— Solid Earth and Planets, v. 90, p. 5513–5521.

Pruess, K., J. Garcia, T. Kovscek, C. Oldenburg, J. Rutqvust, C. Steefel, and T. Xu, 2002, Intercomparison of numerical simulation codes for geological disposal of CO_2: LBNL-51813, p. 86.

Raleigh, C. B., J. H. Healy, and J. D. Bredehoeft, 1976, Experiment in earthquake control at Rangely, Colorado: Science, v. 191, p. 1230–1237.

Sminchak, J. R., and N. Gupta, 2003, Aspects of induced seismic activity and deep-well sequestration of carbon dioxide: Environmental Geosciences, v. 10, p. 81–89.

Span, R., and W. Wagner, 1996, A new equation of state for carbon dioxide covering the fluid region from the triple-point temperature to 1100 K at pressures up to 800 MPa: Journal of Physical and Chemical Reference Data, v. 25, p. 1509–1596.

Townend, J., and M. D. Zoback, 2000, How faulting keeps the crust strong: Geology, v. 28, p. 399–402.

van Genuchten, M. T., 1980, A closed-form equation for predicting the hydraulic conductivity of unsaturated soils: Soil Science Society of America Journal, v. 44, p. 892–898.

White, M. D., N. Gupta, M. E. Kelley, and J. R. Sminchak, 2005, Assessment of CO_2 injection and monitoring strategies at the Mountaineer power plant site using scalable numerical simulation, *in* E. S. Rubin, D. W. Keith, and C. F. Gilboy, eds., Proceedings of the 7th International Greenhouse Gas Control Technologies (GHGT-7) Conference, Volume IIb: Vancouver, Canada, Elsevier, p 2269–2272.

Zoback, M. D., and H. P. Harjes, 1997, Injection-induced earthquakes and crustal stress at 9 km depth at the KTB deep drilling site, Germany: Journal of Geophysical Research— Solid Earth, v. 102, p. 18,477–18,491.

Zoback, M. D., and M. L. Zoback, 1989, Tectonic stress field of the conterminous United States: Geological Society of America Memoir 172, p. 523–539.

Zoback, M. D., D. Moos, L. Mastin, and R. N. Anderson, 1985, Wellbore breakouts and in situ stress: Journal of Geophysical Research— Solid Earth and Planets, v. 90, p. 5523–5530.

Zoback, M. D., C. A. Barton, M. Brudy, D. A. Castillo, T. Finkbeiner, B. R. Grollimund, D. B. Moos, P. Peska, C. D. Ward, and D. J. Wiprut, 2003, Determination of stress orientation and magnitude in deep wells: International Journal of Rock Mechanics and Mining Sciences, v. 40, p. 1049–1076.